

Research Article

Polymer Blend Containing MoO₃ Nanowires with Antibacterial Activity against *Staphylococcus epidermidis* ATCC 12228

Urška Gradišar Centa ¹, Petra Kocbek ², Anna Belcarz ³, Srečo D. Škapin ⁴,
and Maja Remškar ¹

¹Condensed Matter Physics Department, Jožef Stefan Institute, Jamova 39, SI-1000 Ljubljana, Slovenia

²University of Ljubljana, Faculty of Pharmacy, Ljubljana, Slovenia

³Medical University of Lublin, Chair and Department of Biochemistry and Biotechnology, Chodźki 1 Street, 20-093 Lublin, Poland

⁴Advanced Materials Department, Jožef Stefan Institute, Jamova 39, SI-1000 Ljubljana, Slovenia

Correspondence should be addressed to Urška Gradišar Centa; urska.gradisar@ijs.si

Received 3 March 2020; Revised 11 June 2020; Accepted 17 June 2020; Published 6 July 2020

Academic Editor: Angelo Taglietti

Copyright © 2020 Urška Gradišar Centa et al. This is an open access article distributed under the Creative Commons Attribution License, which permits unrestricted use, distribution, and reproduction in any medium, provided the original work is properly cited.

Antibacterial activity of a polymer nanocomposite containing water-soluble poly(ethylene oxide) (PEO), water insoluble poly(vinylidene fluoride-co-hexafluoropropylene) (PVDF-HFP), and MoO₃ nanowires or MoO₃ microparticles as antibacterial active substances is reported. The UV-vis absorption method was used for the illumination of dissolving of the MoO₃ particles of different size and morphology in water. Dissolving of MoO₃ nanowires (1 mg ml⁻¹) decreases pH below 3.6 in only 3 min and below 3 in 15 min, while dissolving of the PEO/PVDF-HFP/MoO₃ nanowires coating (5 mg ml⁻¹) decreases pH below 3.6 in 90 min. These coatings completely destroy the *Staphylococcus epidermidis* ATCC 12228 bacterial strain within 3 h. The proposed applications are antibacterial protective coatings of contact surfaces.

1. Introduction

Infected contact surfaces represent a threat for the health of patients, staff, and visitors in hospitals and for people in crowded areas, such as buses, shopping centers, and schools. Antibacterial agents are of exceptional importance for preventing the spread of infectious diseases [1]. However, their abuse has led to the emergence of antibiotic resistance (e.g., methicillin-resistant bacteria *Staphylococcus aureus*, vancomycin-resistant *Enterococcus* species, and Gram-negative microorganisms [2]). As a result, high doses of antibiotics are necessary for treatment, which can cause adverse side effects [1]. Bacteria have developed antibiotic resistance against many common antibiotics, driving a need to develop alternative strategies to treat bacterial diseases. Gram-positive and Gram-negative bacteria differ in the composition of their cell walls. While the cell wall of Gram-negative bacteria contains a peptidoglycan monolayer and lipopolysaccharide layer called the outer membrane, the cell

wall of Gram-positive bacteria is composed of several layers of peptidoglycan. If nanomaterials directly interact with bacterial species, then, a membrane stress mechanism occurs [3] in which cell death can result from an elevated level of reactive oxygen species (ROS) following the oxidative stress mechanism.

Various nanomaterials have been investigated as promising antibacterial agents (e.g., titanium dioxide, zinc oxide, copper oxide, silver and gold nanoparticles, molybdenum, and tungsten oxides, among others [1, 2]). These nanostructured inorganic materials must satisfy specific rules regarding morphology, size, surface charge, chemical, and physical properties that exhibit antibacterial properties [2]. The mechanism of cellular uptake of nanoparticles (NPs) and their distribution depends mainly on the physicochemical properties of the particles [4]. Several mechanisms of toxicity against bacteria are proposed, including the attachment of NPs to the bacterial membrane by electrostatic interaction, chemical or physical disruption of the membrane, formation

of free radicals (reactive oxygen species-ROS), or induction of frameshift mutations in bacterial strains [1]. As examples, silver ions released from silver NPs affect the surface electric charge of the bacterial membrane and change its penetrability [5]. Similarly, zinc ions released from ZnO NPs damage the bacterial cell membrane and depress the activity of some membranous enzymes [6]. TiO_2 [7] and ZnO [8] NPs cause photocatalytic degradation of the bacteria cell wall and cytoplasmic membrane through production of ROS [6]. Iron oxide NPs can penetrate the cell membrane and damage macromolecules, including DNA, lipids, and proteins, leading to bacterial death [8].

Molybdenum as an element does not show any antimicrobial function. It is one of the essential trace elements of primary importance to humans, and it acts as a cofactor for various enzymes (aldehyde, xanthine, and sulphite oxidase) [9]. The molybdenum trioxide (MoO_3) was reported as a highly promising antibacterial nanomaterial [2, 10, 11]. The antimicrobial principle of MoO_3 in the presence of water is explained by a dissolving process, wherein the acidic reaction with the formation of hydronium (H_3O^+) and molybdate (MoO_4^{2-}) ions occurs [10]. The diffusion of H_3O^+ ions through the bacteria cell wall causes imbalance in the pH equilibrium as well as in the enzyme and transport system of the cell [10]. The acidic low-pH environment caused by dissolving of MoO_3 nanoparticles has been reported as a universal antimicrobial agent against susceptible and resistant isolates of bacterial species causing a hospital-acquired infections [12]. Incorporation of MoO_3 into polymer coatings enables a controlled solubility and a long-term use of such coatings. Zollfrank et al. [11] found the removal or complete inactivation of pathogenic bacteria *S. aureus* and *P. aeruginosa* 3 h after a roll-on test performed with polyurethane tubes filled with MoO_3 and acrylic resin. Piçarra et al. have reported on antibacterial activity of MoO_3 incorporated into diethylenetriamine (SiDETA) against *S. aureus* in comparison with more efficient silver additive [13]. Shafaei et al. [2] reported the influence of different MoO_3 crystalline structures incorporated in various polymer composites on antibacterial activity against *S. aureus*, *E. coli*, and *P. aeruginosa*. The roll-on test showed that all crystalline phases exhibited antimicrobial activity against all three bacteria with elimination in 3 to 9 h. In particular, the orthorhombic phase of MoO_3 prepared by calcination at 300°C exhibited the best efficiency. The antibacterial efficiency depending on a particular MoO_3 crystallographic phase was explained by a need of direct contact between the metal oxide NPs and *E. coli* bacteria, with a contact surface area smaller in a case of hexagonal phase. While both orthorhombic and hexagonal phases of MoO_3 have antibacterial activity against Gram-positive bacteria (*Streptococcus aureus* and *Bacillus megaterium*), antibacterial activity against Gram-negative bacteria *E. coli* was found only for the orthorhombic phase [3]. On the other hand, Kumar Sen et al. report that hexagonal nanorods exhibited better antibacterial activity than nanoplates and that the antimicrobial activity was decreasing with increasing crystallite size [14]. The antibacterial activity against *S. aureus* was found dependent also on energy gap of MoO_3 nanorods [15]. In all these studies, the solubility of

MoO_3 is of a critical importance. Solubility of micrometer sized MoO_3 in water at neutral pH is $56.0 \pm 0.1 \text{ mg ml}^{-1}$ [16].

Here, we present polymer nanocomposites consisting of MoO_3 nanowires in the orthorhombic phase incorporated in a mixture of water soluble polymer-poly(ethylene oxide) (PEO) and water insoluble polymer-poly(vinylidene fluoride-co-hexafluoropropylene)-(PVDF-HFP). This particular polymer combination was selected with an aim to create an inhomogeneous structure of the coating with PEO domains surrounded by inert PVDF-HFP host matrix [17]. A high specific surface area of unique MoO_3 nanowires enables their fast dissolving. Their incorporation into matrix, which is composed of one slowly dissolving and one inert polymers, represents an interesting combination for quick but lasting antibacterial activity, which was not studied yet. The antimicrobial activity of the selected nanocomposite films was assessed against the *Staphylococcus epidermidis* ATCC 12228 bacterial strain, which is nowadays the most frequent cause of nosocomial infections and represents the most common source of infections on indwelling medical devices [18]. The morphology and crystal structure of as-grown MoO_3 nanowires and of the polymer nanocomposite films are shown together with the kinetics of their dissolution in water, which explains the exceptionally fast elimination of the bacteria. Some results are compared with those obtained on commercial (Sigma-Aldrich) MoO_3 and on MoO_3 crystals, both of micrometer size with much smaller specific surface areas.

2. Materials and Methods

2.1. Synthesis of MoO_3 Particles. Three types of MoO_3 particles were used for the comparative studies: nanowires, small microparticles, and larger microparticles. They differ in morphology and specific surface area. The MoO_3 nanowires and small microparticles were synthesized from $\text{Mo}_6\text{S}_2\text{I}_8$ nanowires (Nanotul Ltd.). When these nanowires were oxidized at 285°C for 24 h, the resulting MoO_3 product ($\text{MoO}_3@285$) maintained a nanowire shape and contained a high degree of porosity [19]. Some of the particles were nanotube-like with faceted and polycrystalline walls. On average, the needle-like particles were around 200 nm in diameter and up to $3 \mu\text{m}$ in length (Figure 1(a)). The specific surface area was $12.06 \pm 0.05 \text{ m}^2/\text{g}$. Oxidation of the $\text{Mo}_6\text{S}_2\text{I}_8$ nanowires at 600°C for 6 h led to a growth of MoO_3 monocrystalline particles ($\text{MoO}_3@600$) with a typical size of 2-3 μm , which showed a tendency to form large agglomerates up to $10 \mu\text{m}$ in size (Figure 1(b)). The specific surface area was $1.89 \pm 0.05 \text{ m}^2/\text{g}$. In the comparative study, commercially available MoO_3 (Sigma-Aldrich) crystals with an average size of single crystals of 8-10 μm and clearly visible (001) growth terraces were used (Figure 1(c)). The specific surface area of the crystals (Sigma-Aldrich) was $0.27 \pm 0.05 \text{ m}^2/\text{g}$.

The XRD spectra of the $\text{MoO}_3@285$, $\text{MoO}_3@600$, and MoO_3 (Sigma-Aldrich) particles presented in Figure 2 show that all three types of particles grew in the orthorhombic crystal structure (JCPD 76-1003). The positions of the peaks all belong to the orthorhombic phase match in all spectra, while widths of the peaks are widened with reduction of the

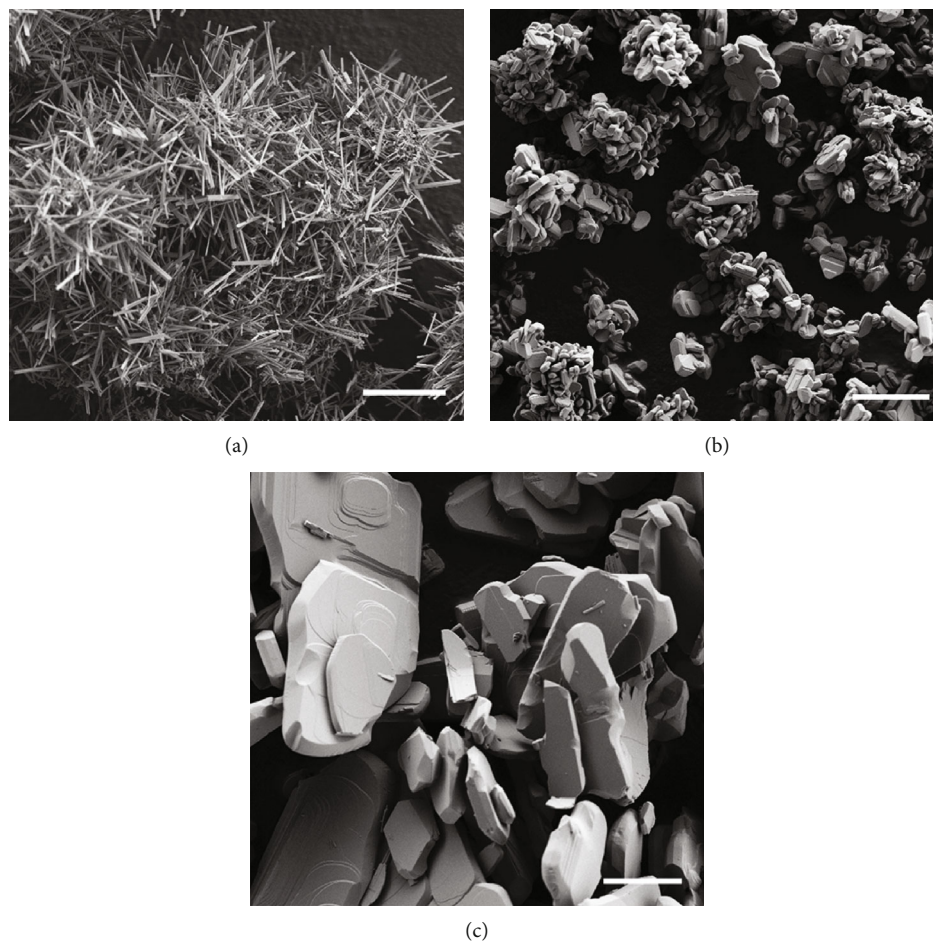


FIGURE 1: SEM images of the nanomaterials: (a) $\text{MoO}_3@285$, (b) $\text{MoO}_3@600$, and (c) MoO_3 (Sigma-Aldrich). Scale bar: $10\ \mu\text{m}$.

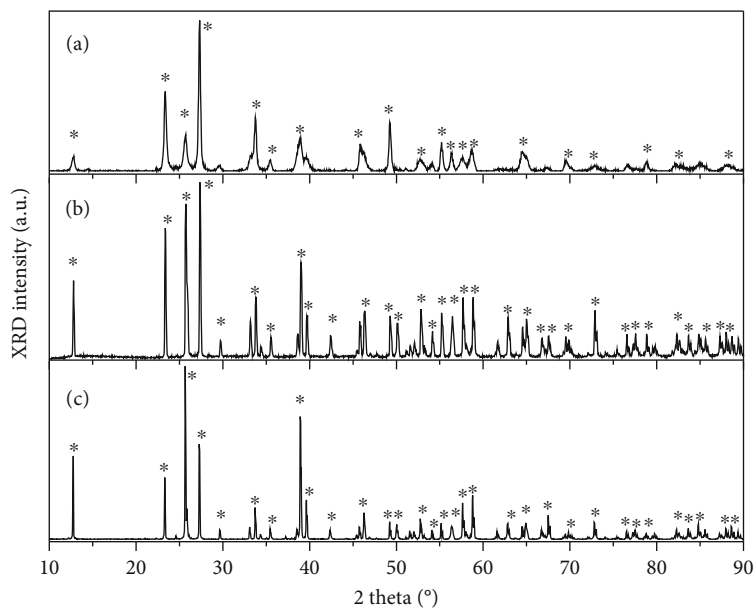


FIGURE 2: XRD spectra: (a) $\text{MoO}_3@285^\circ\text{C}$; (b) $\text{MoO}_3@600^\circ\text{C}$; (c) MoO_3 (Sigma-Aldrich).

particle size. Variations in the relative intensity of the peaks in the spectrum shown in Figure 2(a) in comparison with the spectra shown in Figures 2(b) and 2(c) are due to the anisotropic shape of the MoO₃@285 nanowires.

The polymers, PVDF-HFP (average $M_w \approx 400,000$) and PEO (average $M_w \approx 900,000$), both purchased at Sigma-Aldrich, were separately dissolved in dimethylformamide (DMF) ($M_w = 73.09$) (Acros Organics) at concentrations of 18% and 3%, respectively. The coatings were prepared using different mixing procedures and with different sizes of the MoO₃ particles (Table 1). The same mass ratio of 69:23:8 (PVDF-HFP:PEO:MoO₃) was used for all coatings, which were prepared as self-standing thin films. The average film thickness of $44 \mu\text{m} \pm 4 \mu\text{m}$ was determined from optical images.

2.2. Preparation of the MoO₃ Polymer Nanocomposites.

Parameters of the film preparation are listed in Table 1. The polymer solutions for all nanocomposite films were prepared in the same way; i.e., PVDF-HFP and PEO were separately dissolved in DMF at room temperature (RT) under mixing on the magnetic stirrer (300 rpm) for two hours.

With the aim to understand the influence of MoO₃ environment on its solubility, the MoO₃ nanoparticles were inserted either firstly to PEO only (Step 1) and then both components were in Step 2 mixed with PVDF-HFP (all films but film D), or added directly to previously mixed PEO/PVDF-HFP (film D). All mixtures were stirred for additional 30 min. Such created nanocomposite dispersions were casted into a glass Petri dish and dried at 80°C for 2 h. The effect of temperature during polymer dissolving was investigated in film B, which was prepared all the way at 80°C. To avoid large MoO₃ agglomerates, which sized up to 20 μm in films A and B, the MoO₃@285 was dispersed in acetone ($M_w = 58.08$, Merck) in 0.5 wt.% and allowed to sediment for 2 min. Dried material from the supernatant called (MoO₃@285-N) was used in the films C and D. With the aim to resolve the effect of MoO₃ and its crystalline size on antibacterial activity, film E without MoO₃ was prepared and film F with added large MoO₃@600 particles. For comparison with commercially available MoO₃, film G was made using MoO₃ purchased at Sigma-Aldrich.

The SEM micrographs (Figure 3) show the topography of films A–D (Table 1) prepared with MoO₃@285 particles. Films A and B are continuous and show a typical domain structure; however, this structure is smaller in film B which was prepared at 80°C. Films C and D, which were prepared with material without large agglomerates, have some surface depression appeared due to the rapid evaporation of DMF during film drying. Their appearance is stochastic, but relatively rare. In most cases, agglomerates of MoO₃ particles are visible inside the holes or in their vicinity. While film C has a similar domain size as in films A and B and does not contain agglomerates, film D has approx. 10 times larger domains and the presence of MoO₃@285 agglomerates, which formed in the mixture of PEO and PVDF-HFP.

2.3. *Methods.* Powder X-ray diffraction (XRD) of the MoO₃ nanomaterials was performed at room temperature

(RT) with a D4 Endeavor diffractometer (Bruker AXS) using a quartz monochromator Cu K α radiation source ($\lambda = 0.1541 \text{ nm}$) and a Sol-X dispersive detector. The range of 2θ was chosen from 7° to 95° with a step size of 0.04°. A specific surface area of MoO₃ nanotubes and microcrystals was measured by the BET method (Gemini II 2370, Surface Area Analyzer, Micromeritics, USA). The morphology of the nanoparticles and composite films put on an adhesive carbon tape was investigated using a field emission scanning electron microscope (SEM) (Supra 36 VP, Carl Zeiss). The films were sputtered with a 10 nm layer of gold for better conductance. UV-vis spectroscopy was performed using a Perkin Elmer spectrometer Lambda 950 using a quartz cuvette.

The concentration of dissolved MoO₃ was determined using UV-vis spectroscopy. For calibration, the value of the absorbance peak at 215 nm in several MoO₃-water solutions with known concentrations was measured.

The SevenExcellence Multiparameter (Mettler Toledo) with probe InLab Expert Pro-ISM was used for measuring pH values, and an InLab 731-ISM was used to measure conductivity. The measurements of pH values and conductivity of the solution were sampled in 1-minute time intervals for MoO₃@285, MoO₃@600, and MoO₃ (Sigma-Aldrich) dissolving in water at a concentration of 1 mg/ml at room temperature. Each pH measurement has started with a few measurements of pure water to determine the base pH level, after which point the MoO₃ was inserted. Different base levels revealed a degree of pH value variations in pure water. Between individual measurements, the samples in glass beakers were mixed with a magnetic stirrer at 400 rpm.

For dissolving kinetics of the MoO₃ particles, the MoO₃@285, MoO₃@600, and MoO₃ (Sigma-Aldrich) crystals were dissolving in water at room temperature in a concentration of 1 mg/ml. The pH values and conductivity of the solutions were measured in 1-minute intervals. Each pH measurement started with measuring of pure water with the aim to determine the base pH level variations. The solutions were mixed with a magnetic stirrer at 400 rpm between individual measurements.

For measurements of dissolving kinetics of the MoO₃-based nanocomposite films, they were dissolving in water at room temperature in a concentration of 5 mg/ml. The pH values of the solutions were measured in 5 min intervals and mixed between individual measurements with a magnetic stirrer at 400 rpm.

Antibacterial activity of the PVDF-HFP/PEO polymer films was evaluated according to Japanese Industrial Standard (JIS) Z 2801:2000: antimicrobial products test for antimicrobial activity and efficacy. This standard is designed to evaluate the antimicrobial activity and efficacy on bacteria of antimicrobial product surfaces and is applicable to plastic, metal, and ceramic products. Prior to testing, the polymer films (approx. 7 cm in diameter, 50 μm thick) were UV-sterilized (30 min per each side), which caused curvature of the films. The standardized method was therefore modified to avoid leakage of the inoculate from the curved films by applying the inoculate onto a piece of sterile Whatman paper placed onto the film and not directly onto the tested film. The tested films with inoculum were placed between two pieces of

TABLE 1: The MoO₃ particles and synthesis parameters of the films.

Film	Nanoparticles	Media 1/temperature (°C) Step 1	Media 2 Step 2
A	MoO ₃ @285	PEO/RT	PVDF-HFP
B	MoO ₃ @285	PEO/80	PVDF-HFP
C	MoO ₃ @285-N	PEO/RT	PVDF-HFP
D	MoO ₃ @285-N	PEO+PVDF-HFP/RT	
E	/	PEO/RT	PVDF-HFP
F	MoO ₃ @600	PEO/RT	PVDF-HFP
G	MoO ₃ (Sigma-Aldrich)	PEO/RT	PVDF-HFP

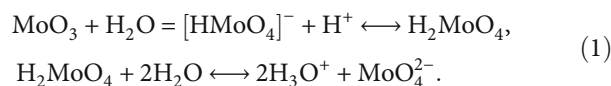
inert polymeric foil and then inserted between two rigid titanium plates to stabilize the films and protect both against water evaporation and contact with titanium. A clean and UV-sterilized polypropylene foil sandwich with an inoculum-soaked piece of Whatman paper inside was used as a control. A reference bacterial strain from the American Type Culture Collection, *Staphylococcus epidermidis* ATCC 12228, was maintained as stock in sterile Microbanks (Technical Service Consultants Limited, UK) at -20°C. Before the experiment, the bacteria were transplanted onto fresh slant culture medium (Mueller-Hinton Agar) and cultured for 20-24 h at 37°C. Cultured bacteria were transferred into liquid medium (Mueller-Hinton Broth), incubated for 20-24 h at 37°C, centrifuged, and suspended in 500-fold diluted Mueller-Hinton Broth directly before the experiment, at an approximate density of 6×10^8 . On the Whatman paper, 40 μ l inoculum was applied per 1 cm² film surface. All samples were incubated with bacterial inoculate for 3 h, 6 h, and 24 h at 37°C. After incubation, the bacteria were eluted from the samples and Whatman papers by shaking in 5 ml 0.9% NaCl for 1 min. The pH of the obtained extract was measured using an HI 8010 pH meter (Hanna Instruments, Romania). The number of eluted viable bacterial cells was quantified using the serial dilution method after 24 h of growth at 37°C on Mueller-Hinton agar plates. The experiments were performed in triplicate, and the mean and standard deviation (SD) values were calculated using Excel 2016.

3. Results

3.1. Dissolving Kinetics of the MoO₃ Particles. Figure 4(a) shows the pH curves of dissolving process of first 300 min for all three used MoO₃. The MoO₃@285 dissolved the quickest. In only 3 min, the pH dropped below 3.5 and in 15 min below 3. This fast dissolving caused a quick increase of conductivity in the solution (Figure 4(b)—curve A). This is consistent with the larger specific surface area of MoO₃@285 in comparison with MoO₃@600 and MoO₃ (Sigma Aldrich), which both dissolved at a slower rate, with the conductivity of these solutions increasing semilinearly in the first 3 h (Figure 4(b)—curves B and C).

The time evolution of the dissolving process is shown via absorption of UV-vis light in Figure 5. The dissolution dynamics of MoO₃@285 and MoO₃@600 are affected by a specific surface area, oxygen deficiency in MoO₃@285, and

the presence of individual molybdate species. The surface of MoO₃ nanoparticles in contact with water starts to dissolve in the following way [20]:



Simultaneously, the protonation process of the molybdate ions (MoO₄²⁻) takes place:



Figure 5 shows the UV-vis spectrum of MoO₃@285 solution at different times after addition of the material into the water (5, 10, 30, 90, and 180 min). After 5 min, two peaks were observed with relatively low but comparable intensities. They were centered at 213 nm (peak I) and 231 nm (peak II), indicating that the dissolving had started. The peaks are explained as absorption by the heptamolybdate ions Mo₇O₂₄⁶⁻ (212 nm), their double protonated form H₂Mo₇O₂₄⁴⁻ (238 nm), and presence of MoO₄²⁻ (207 nm and 228 nm) [21]. In the first 10 min, the peaks and absorption tail at wavelengths larger than 260 nm were increasing. The tail indicates the transitional formation of molybdic acid [22] and its protonated monomers HMoO₄⁻ [23, 24]. Later, the tail intensity was decreased, indicating that the solution established a stationary phase where a mixture of monomers MoO₄²⁻ and H₂Mo₇O₂₄⁴⁻ were dominant. After 30 min, the positions of both peaks stabilized at 213.5 nm and 229.5 nm for Peak I and Peak II, respectively. The isosbestic point for MoO₃@285, where the total absorption does not change during a chemical reaction, occurs at 245 nm.

Figure 5(b) shows the time evolution of the UV-vis spectrum of the MoO₃@600 solution at 5, 10, 30, 90, and 180 min of dissolving. In contrast with MoO₃@285, the absorption at wavelengths above 250 nm increased over the time to the end of the experiment indicating that the concentration of MoO₄²⁻ monomers was still increasing. The protonation process of the molybdate ions was not observed, and the basic shape of UV spectra did not change with time. The isosbestic point was not present.

3.2. Dissolving Kinetics of the MoO₃-Based Nanocomposite Films. The films begin to dissolve very quickly. In 10 min,

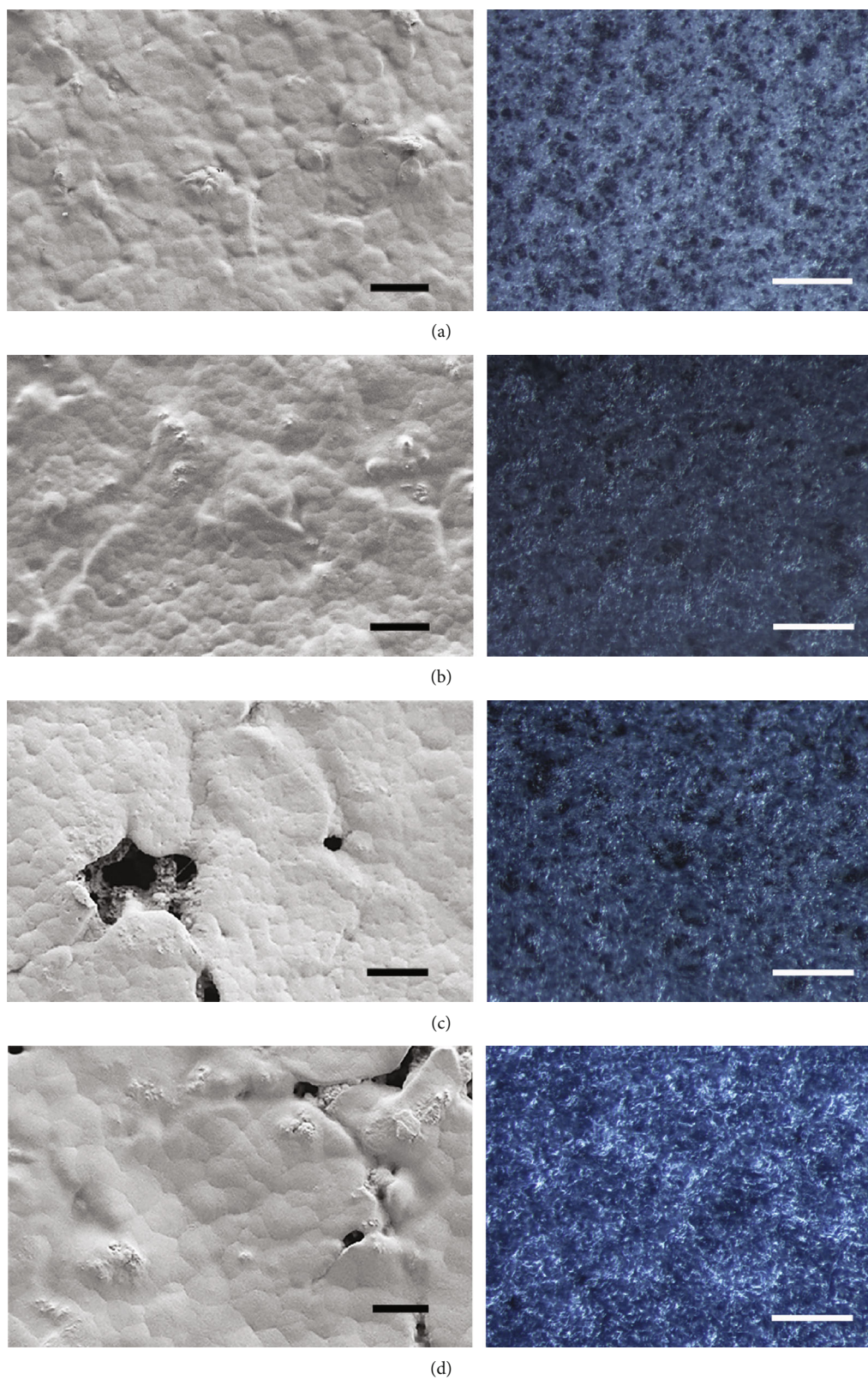


FIGURE 3: Left: SEM images of surface topography of films containing $\text{MoO}_3@285$ nanoparticles ((a) film A prepared at room temperature; (b) film B prepared at 80°C ; (c) film C prepared from size purified particles; (d) film D prepared by insertion of size purified particles into a polymer mixture). Scale bar: $20\ \mu\text{m}$. Right: optical images of the same films. Scale bar: $200\ \mu\text{m}$.

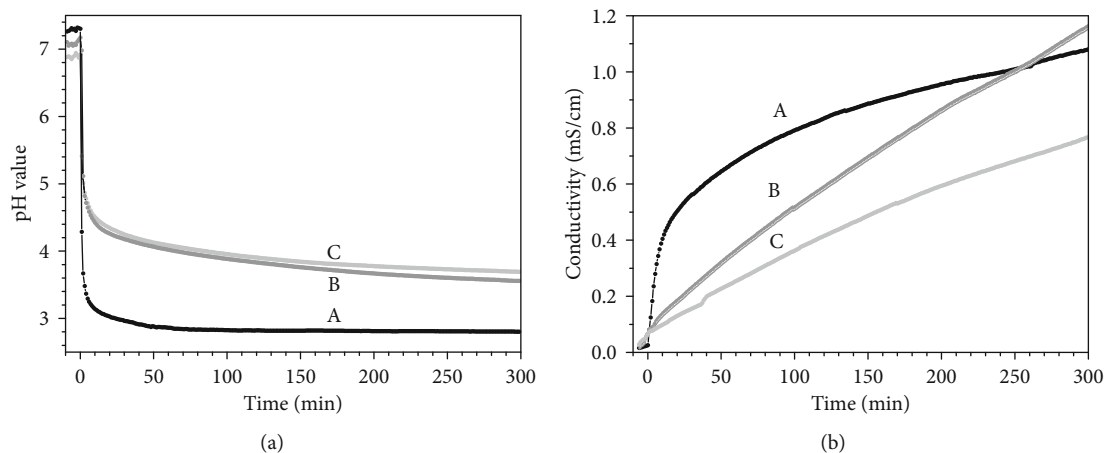


FIGURE 4: (a) pH values of the water solutions by time; (b) conductivity of the water solutions: A— $\text{MoO}_3@285$ nanoparticles; B— $\text{MoO}_3@600^\circ\text{C}$ microparticles; C— MoO_3 (Sigma-Aldrich).

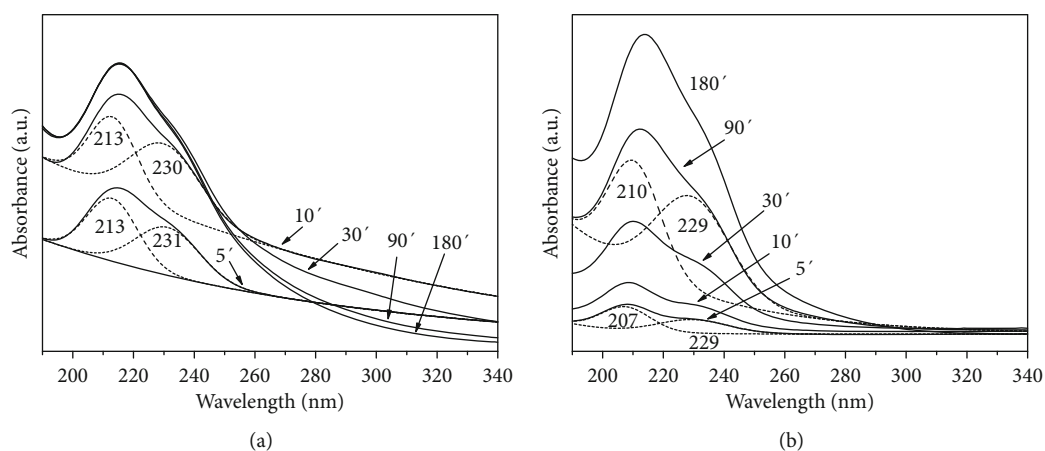


FIGURE 5: Time dependency of UV-vis absorption during MoO_3 dissolving in water at concentration of 0.06 mg/ml: (a) $\text{MoO}_3@285$; (b) $\text{MoO}_3@600$.

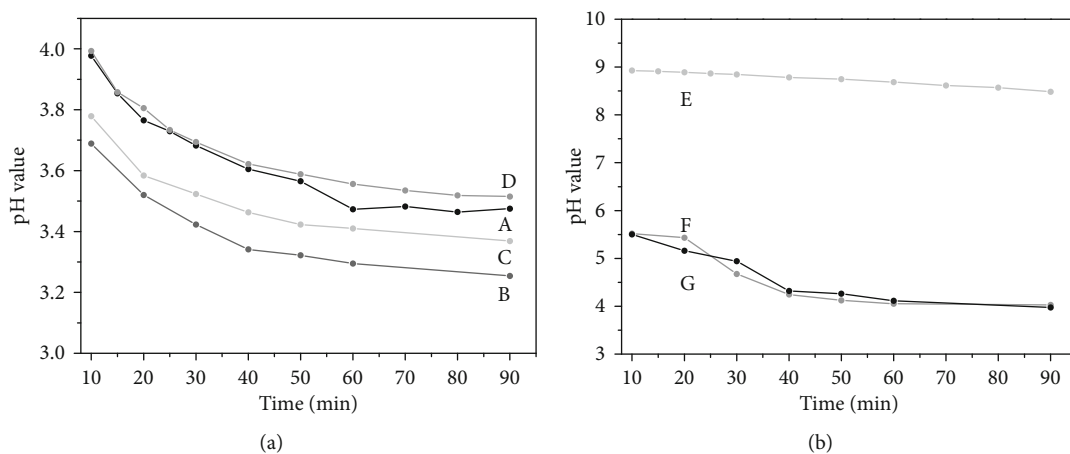


FIGURE 6: Time dependency of pH values during dissolution of MoO_3 from PEO/PVDF-HFP films in deionized water: (a) films A-D containing $\text{MoO}_3@285$ nanoparticles; (b) film E without MoO_3 , film F containing $\text{MoO}_3@600$ micro particles, and film G containing commercial MoO_3 particles (Sigma Aldrich).

the pH values dropped below 4 (Figure 6(a)) for all four films containing $\text{MoO}_3@285$ nanoparticles (AD: Table 1). In comparison, the first measurements 10 min after film insertion into water showed identical pH values for films A and D (pH~4), a lower value for film C (pH~3.8), and the lowest value for film B (pH~3.7). In 90 min, only film A reached the saturated value of 3.45, while the pH values of the other films were still decreasing. The lowest pH value (3.25) was achieved for film B, which was prepared with PEO dissolved at 80°C, while the highest pH value was 3.5 for film D prepared by the one-step method.

From the similar pH values of films A and D, one can conclude that agglomeration of the primary particles decreased the solubility rate regardless of the local environment and that the order of the mixing of the polymers did not substantially affect the solubility. A higher temperature of the mixing (film B) caused faster dissolution and therefore smaller pH value.

The solubility of the coating without MoO_3 (film E) only slightly reduced the pH value (from 9 to 8.5) due to weak PEO dissolving, which was still in progress at the end of the selected time period of 90 min. Dissolution of films F and G, which contained larger $\text{MoO}_3@600$ and MoO_3 (Aldrich) particles, respectively, decreased the pH value below 5 in 25 min, but the final pH value did not decrease below 4.2 (Figure 6(b)).

Concentrations of the dissolved MoO_3 by time are shown in Figure 7. The first measurement 5 min after insertion of the films into water showed identical concentrations for films A and B, which have similar surface topography (Figures 3(a) and 3(b)), while concentrations of the dissolved MoO_3 from films C and D, which are porous, were higher. The highest concentration was measured for film D, which contained exposed agglomerates of MoO_3 . After 90 min of dissolving, films A, B, and D, which all contained MoO_3 agglomerates, were dissolved to nearly equal amounts (0.15–0.16 mg/ml), while film C, which contained highly dispersed MoO_3 nanoparticles, was less dissolved (0.12 mg/ml). A relatively slow dissolution of film C is explained by the slow dissolution of PEO, which covered the MoO_3 single nanoparticles more efficiently than their agglomerates, and prevented contact with water.

3.3. Antibacterial Activity of the $\text{MoO}_3/\text{PVDF-HFP}/\text{PEO}$ Films. Antibacterial activity of films A, D, and E was tested against the *Staphylococcus epidermidis* ATCC 12228 (Gram-positive) bacterial strain. Films A and D were selected because of their high solubility and assumption that the local environment of MoO_3 particles was different in both films. In film A, which was prepared by mixing MoO_3 with PEO and then with PVDF-HFP, MoO_3 is more likely to be surrounded by water soluble PEO than in film D. Film E, without MoO_3 , was used as a reference, while the inoculate incubated with inert polypropylene films was used as a positive control.

Results are shown in Figure 8. The main result is that the antibacterial activity of both films A and D containing $\text{MoO}_3@285$ nanoparticles is high. Only 3 h after incubation, no bacteria survived being in contact with the film A and only 0.2% with the film D. A prolonged time of the contact

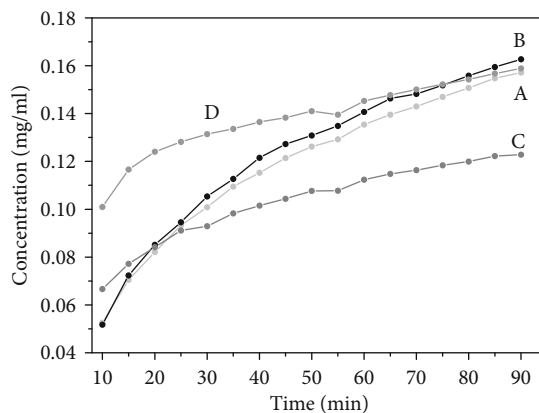


FIGURE 7: Time evolution of the concentration of dissolved MoO_3 from films A-D.

(6 h and 24 h) causes a complete elimination of alive bacteria being in contact with any of film A or D.

During incubation of the tested films with bacterial inoculate, partial dissolution of water-soluble PEO and MoO_3 particles was expected to appear and cause the acidic environment. Therefore, pH values in extracts collected from the films, which were incubated for 3, 6, and 24 h with bacterial inoculate, were measured over time. The results are presented in Table 2. Extracts collected from the control and the reference samples exhibited pH values of 5.2–5.3 and 5.2–5.4, respectively. However, for extracts collected from both A and D films, the pH values were much lower: 1.7–1.8 measured 3 h after incubation and 1.54–1.60, 6 h after incubation.

In contrast, an increase of bacterial CFU (colony forming unit) on reference film E (without MoO_3) in comparison with the control film was observed (Figure 8). Three hours after incubation with bacterial inocula, the CFU increased to 243% of the control and in 6 h to 660% of the control. After 24 h, this effect disappeared—only 15% of cells survived in contact with film E in comparison with the control.

4. Discussion

The growth of bacteria and fungi slowed down at pH values between 3.5 and 4 for many types of bacteria (e.g., staphylococci, streptococci, enterococci, *Legionella pneumophila*, *Lactobacillus acidophilus* spp., *Candida* spp., and *Aspergillus* spp.) [11]. The majority of microorganisms are effectively killed at pH values 3.5–4.0, but many Gram-negative microorganisms are killed at higher pH values up to 5.5 (*E. coli*, *Pseudomonas aeruginosa*, *Clostridia*, and *Campylobacter*) [11]. The PVDF-HFP/PEO/ MoO_3 nanocomposite dissolves in water to a sufficient degree such that the dissolved MoO_3 locally reduces the pH values below 3.6, consequently providing an effective antimicrobial environment.

The dissolution process of orthorhombic crystalline phase MoO_3 particles of different sizes and specific surface areas was studied for their potential application in antimicrobial polymer nanocomposites. The smallest MoO_3 nanoparticles synthesized from $\text{Mo}_6\text{S}_2\text{I}_8$ nanowires dissolved the

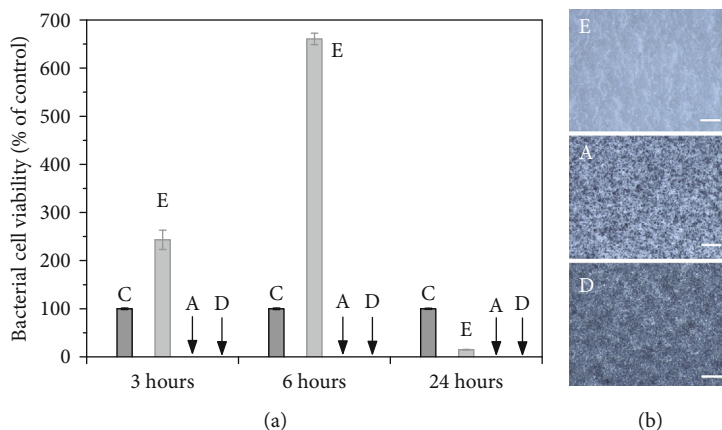


FIGURE 8: (a) Bacterial cell viability (as % of the control), 3, 6, and 24 h after exposure of the *S. epidermidis* ATCC 12228 bacterial strain with polymer films. C: control; E: reference film without MoO₃; A and D: films containing MoO₃@285 nanoparticles prepared according to the 2-step method and 1-step method, respectively. (b) Optical images of tested films. Scale bars: 200 μm.

TABLE 2: Changes of pH in the extract from tested polymer films incubated for 3, 6, and 24 h with *S. epidermidis* inoculate.

Sample	3 h	pH 6 h	24 h
Control	5.22 ± 0.01	5.20 ± 0.10	5.27 ± 0.01
E	5.19 ± 0.03	5.37 ± 0.01	5.21 ± 0.01
A	1.84 ± 0.02	1.54 ± 0.02	1.61 ± 0.01
D	1.72 ± 0.04	1.60 ± 0.01	1.59 ± 0.02

fastest. Nanoparticles with a specific surface area of approx. 12 m²/g dissolved in water to a concentration of 1 mg/ml, dropping the pH value below 3.5 in 1 min and below 3 in 15 min. The exponential decrease of pH value with time and the related exponential enhancement of conductance provide evidence of a very fast dissolving process. The time dependencies of pH and conductance (Figure 4) were fitted for the first 45 min of the dissolving process with biexponential curves ($y = A_1 \cdot \exp(-x/t_1) + A_2 \cdot \exp(-x/t_2) + y_0$) with two different time constants. For the pH curve, they are $t_1 = 166$ min, $t_2 = 5$ min, with A_1 and A_2 of -908 and -421 mS/cm, while for the conductance curve, they are $t_1 = 2$ min and $t_2 = 18$ min, and A_1 and A_2 are -414 and -627 mS/cm, respectively. The adjusted R -square of the pH curve fit is 0.997 and of the conductance fit is 0.9994. Consequently, the UV-vis absorbance of the dissolving MoO₃@285 reached a stationary state in 90 min, while the absorbance of the dissolved MoO₃@600 increased semilinearly with time and the stationary phase was not reached within 3 h. The UV-vis spectroscopy of the MoO₃@285 solution indicated the presence of [HMoO₄]-monomers (protonated form of molybdic acid) in the first 10 min and their reduction to MoO₄²⁻ monomers, while the protonation reaction in the case of MoO₃@600 continued up to the end of the experiment and the isosbestic point was not observed.

The PVDF-HFP/MoO₃ nanocomposites were prepared as thin films in various ways with the aim to test how size

of the MoO₃ particles, the order of mixing polymers, and different preparation temperatures influence composite solubility. Due to the different solubility rates of the MoO₃ particles and their aggregates, different final pH values were obtained within the 90 min dissolution testing period in water. All the films containing MoO₃@285 nanoparticles decreased the pH value of the water solution below 4 in only 10 min (Figure 4(a)), while larger MoO₃@600 and MoO₃ (Aldrich) decreased the pH value below 4 in 60 min. The lowest pH value (3.2) was obtained with film B, prepared at 80°C, where the enhanced temperature increased the dispersion of the polymers (Figure 6(a)).

The highest concentration of dissolved MoO₃ after 90 min was 0.16 mg/ml. The concentration increased the fastest during dissolution of film D, which was prepared using a one-step procedure which involved mixing MoO₃@285 directly into the mixture of PVDF-HFP and PEO. Because both polymers segregate during the drying process, the MoO₃ was the most exposed to the water molecules during dissolution.

Two films (A and D) were selected for antibacterial testing because of their high solubility and different local environment of the MoO₃@285 particles. The antibacterial activity of both films was found to be quick and efficient. Film A was slightly more effective, because no bacteria survived after 3 h, and only 0.2% on film D. After 6 h, no live bacteria were found on either film. It seems that the strong antibacterial effect can be attributed to the strongly acidic aqueous environment resulting from their dissolution, as suggested elsewhere [10].

In this study, the antibacterial activity of films was evaluated according to the modified standard designed for solid surfaces. Experimental conditions included incubation of tested films with a Whatman paper soaked in bacterial inoculate. Thus, the humidity of the environment of the incubated sample was very limited. Similar conditions usually appear for handles, handrails, or toilet walls—these surfaces are also rich in bacteria but only slightly moistened. On the basis of our results, it is likely that PEO/PVDF-HFP films

enriched with MoO₃ particles could be used as effective coatings against bacteria deposited on different surfaces in hospitals, buses, schools, and shopping centers. Their application as coatings on handles, handrails, or hospital bed surfaces could limit the risk of infectious microorganism transmission.

Interestingly, for the reference PEO/PVDF-HFP film without MoO₃ particles (film E), the initial stimulation of bacterial growth was observed. Most probably, traces of dissolved PEO or other compounds of reference film served as a nutrient and allowed for the division and propagation of bacterial cells during the initial period of incubation. This was not observed in the case of the control (polypropylene foil), because the inoculum itself contains only traces of nutritious substances and supports the metabolism, but not the propagation, of bacteria. This stimulation was then followed by a significant reduction of bacterial viability after 24 h incubation. The reason for this phenomenon may lie in the decreased humidity of the environment (as inoculum was absorbed by the film) and the increase of osmotic strength, causing the inhibition of cell survivability. Moreover, it was previously noted that PEO itself can exhibit antibacterial action because of its ability to prevent the adsorption of plasma proteins, which is the first step of bacterial adhesion and biofilm formation. Based on this property, PEO coatings showed high potential to prevent *S. epidermidis* adhesion, although stability of the coatings was limited [25]. Therefore, it would be possible that PEO itself contributes to the antibacterial activity of the PEO/PVDF-HFP/MoO₃ films, but the stimulation of the bacterial growth being in contact with the film E, which is without MoO₃, for 3 h and 6 h, denies this assumption. Therefore, the antibacterial activity of the PEO/PVDF-HFP/MoO₃ coatings can be attributed solely to MoO₃.

5. Conclusion

We have formulated polymer nanocomposites intended for application as antimicrobial contact surfaces. The nanocomposites are based on a mixture of chemically inert PVDF-HFP polymer, water-soluble PEO polymer, and MoO₃ particles of different sizes and morphologies as antibacterial material. Exposed to water (1 mg/ml), the MoO₃ nanowires due to their high specific surface area dissolve quickly and decrease pH below 3.6 in only 3 min. The MoO₃ dissolved from the PVDF-HFP/PEO/MoO₃ nanowire composite in water (5 mg/ml) decreases pH below 3.6 in 90 min and completely destroys the *Staphylococcus epidermidis* ATCC 12228 bacterial strain within 3 h.

Data Availability

No data were used to support this study.

Conflicts of Interest

There are no conflicts to declare.

Acknowledgments

This work was financially supported by the Slovenian Research Agency through contracts P0-5544 and P1-0099. The authors thank Mr. J. Jelenc for the technical assistance in the preparation of the polymer nanocomposites.

References

- [1] M. J. Hajipour, K. M. Fromm, A. A. Ashkarran et al., "Antibacterial properties of nanoparticles," *Trends in Biotechnology*, vol. 30, no. 10, pp. 499–511, 2012.
- [2] S. Shafaei, M. Lackner, M. Meier, J. Plank, J. P. Guggenbichler, and C. Zollfrank, "Polymorphs of molybdenum trioxide as innovative antimicrobial materials," *Surface Innovations*, vol. 1, no. 4, pp. 202–208, 2013.
- [3] N. Desai and S. Mali, "Chemically grown MoO₃ nanorods for antibacterial activity study," *Journal of Nanomedicine & Nanotechnology*, vol. 6, no. 6, pp. 338–344, 2015.
- [4] A. Kunzmann, B. Andersson, T. Thurnherr, H. Krug, A. Scheynius, and B. Fadeel, "Toxicology of engineered nanomaterials: focus on biocompatibility, biodistribution and biodegradation," *Biochimica et Biophysica Acta*, vol. 1810, no. 3, pp. 361–373, 2011.
- [5] W. K. Jung, H. C. Koo, K. W. Kim, S. Shin, S. H. Kim, and Y. H. Park, "Antibacterial activity and mechanism of action of the silver ion in *Staphylococcus aureus* and *Escherichia coli*," *Applied and Environmental Microbiology*, vol. 74, no. 7, pp. 2171–2178, 2008.
- [6] N. Padmavathy and R. Vijayaraghavan, "Interaction of ZnO nanoparticles with microbes—a physio and biochemical assay," *Journal of Biomedical Nanotechnology*, vol. 7, no. 6, pp. 813–822, 2011.
- [7] H. A. Foster, I. B. Ditta, S. Varghese, and A. Steele, "Photocatalytic disinfection using titanium dioxide: spectrum and mechanism of antimicrobial activity," *Applied Microbiology and Biotechnology*, vol. 90, no. 6, pp. 1847–1868, 2011.
- [8] L. Wang, C. Hu, and L. Shao, "The antimicrobial activity of nanoparticles: present situation and prospects for the future," *International Journal of Nanomedicine*, vol. Volume 12, pp. 1227–1249, 2017.
- [9] M. Yoshida, H. Hattori, S. Ota et al., "Molybdenum balance in healthy young Japanese women," *Journal of Trace Elements in Medicine and Biology*, vol. 20, no. 4, pp. 245–252, 2006.
- [10] K. Krishnamoorthy, M. Veerapandian, K. Yun, and S. J. Kim, "New function of molybdenum trioxide nanoplates: toxicity towards pathogenic bacteria through membrane stress," *Colloids and Surfaces B: Biointerfaces*, vol. 112, pp. 521–524, 2013.
- [11] C. Zollfrank, K. Gutbrod, P. Wechsler, and J. P. Guggenbichler, "Antimicrobial activity of transition metal acid MoO₃ prevents microbial growth on material surfaces," *Materials Science and Engineering C*, vol. 32, no. 1, pp. 47–54, 2012.
- [12] E. Lopes, S. Piçarra, P. L. Almeida, H. de Lencastre, and M. Aires-de-Sousa, "Bactericidal efficacy of molybdenum oxide nanoparticles against antimicrobial-resistant pathogens," *Journal of Medical Microbiology*, vol. 67, no. 8, pp. 1042–1046, 2018.
- [13] S. Piçarra, E. Lopes, P. L. Almeida, H. de Lencastre, and M. Aires-de-Sousa, "Novel coating containing molybdenum oxide nanoparticles to reduce *Staphylococcus aureus* contamination on inanimate surfaces," *PLoS One*, vol. 14, no. 3, article e0213151, 2019.

- [14] S. K. Sen, S. Dutta, M. R. Khan et al., "Characterization and antibacterial activity study of hydrothermally synthesized h-MoO₃ nanorods and α -MoO₃ nanoplates," *BioNanoScience*, vol. 9, no. 4, pp. 873–882, 2019.
- [15] A. Kumar and G. Pandey, "Synthesis, characterization, effect of temperature on band gap energy of molybdenum oxide nano rods and their antibacterial activity," *American Journal of Applied and Industrial Chemistry*, vol. 3, no. 3, pp. 38–42, 2017.
- [16] P. Venkataramana and V. R. Krishnan, "Solubilities of molybdenum and tungsten trioxides by tracer technique," *Radiochemical and Radioanalytical Letters*, vol. 53, no. 3, pp. 189–194, 1982, <https://ntrs.nasa.gov/archive/nasa/casi.ntrs.nasa.gov/19690030668.pdf>.
- [17] J. Xi, X. Qiu, J. Li, X. Tang, W. Zhu, and L. Chen, "PVDF-PEO blends based microporous polymer electrolyte: effect of PEO on pore configurations and ionic conductivity," *Journal of Power Sources*, vol. 157, no. 1, pp. 501–506, 2006.
- [18] M. Otto, "Staphylococcus epidermidis-the 'accidental' pathogen," *Nature Reviews Microbiology*, vol. 7, no. 8, pp. 555–567, 2009.
- [19] A. Varlec, D. Arčon, S. D. Škapin, and M. Remškar, "Oxygen deficiency in MoO₃ polycrystalline nanowires and nanotubes," *Materials Chemistry and Physics*, vol. 170, pp. 154–161, 2016.
- [20] Z. Minubaeva, "UV spectroscopic studies of the hydrothermal geochemistry of molybdenum and tungsten," *Doctoral dissertation*, ETH Zurich, ETH, 2007.
- [21] J. J. Cruywagen and J. B. B. Heyns, "Equilibria and UV spectra of mono- and polynuclear molybdenum (VI) species," *Inorganic Chemistry*, vol. 26, no. 16, pp. 2569–2572, 1987.
- [22] O. F. Oyerinde, C. L. Weeks, A. D. Anbar, and T. G. Spiro, "Solution structure of molybdic acid from Raman spectroscopy and DFT analysis," *Inorganica Chimica Acta*, vol. 361, no. 4, pp. 1000–1007, 2008.
- [23] T. Ozeki, H. Kihara, and S. Ikeda, "Study of equilibria in 0.03 mM molybdate acidic aqueous solutions by factor analysis applied to ultraviolet spectra," *Analytical Chemistry*, vol. 60, no. 19, pp. 2055–2059, 2002.
- [24] C. V. Krishnan, R. Muñoz-Espí, Q. Li, C. Burger, and B. Chu, "Formation of molybdenum oxide nanostructures controlled by poly(ethylene oxide)," *Chinese Journal of Polymer Science*, vol. 27, no. 1, pp. 11–22, 2009.
- [25] A. Roosjen, J. de Vries, H. C. van der Mei, W. Norde, and H. J. Busscher, "Stability and effectiveness against bacterial adhesion of poly(ethylene oxide) coatings in biological fluids," *Journal of Biomedical Materials Research Part B: Applied Biomaterials*, vol. 73B, no. 2, pp. 347–354, 2005.